Rotary Inductive Power Transfer for LED Lighting Systems

Chung-Chuan Hou, Chia-Ming Chang, Wei-Hsiang Cheng, and Hsien-Ching Huang
Chung Hua University, Hsinchu, Taiwan, R.O.C.

***Abstract*--Rotary inductive power transfer (RIPT) systems have the advantages in wireless power transfer capability, unlimited angular position operation, and flexible light-emitting diode (LED) lighting application. Therefore, this study discusses the performances of RIPT for LED lighting systems in the frequency domain and time domain. The characteristics of the RIPT for LED lighting systems are measured under varied air gap, changed load, and so on. The simulation and experimental results are presented to validate the performances of the proposed scheme.**

***Index Terms*--LED lighting, rotary inductive power transfer, unlimited angular position operation.**

I. Introduction

To this day the rotary inductive power transfer (RIPT) systems [1-4] are expanded quickly due to the advantages of the RIPT are wireless power transfer capability, unlimited angular position operation, and flexible light-emitting diode (LED) lighting application [5]. Figure 1 shows the RIPT for LED lighting system. A DC-AC H-bridge inverter (HBI) is utilized to generate the high frequency square wave voltage (v_{in}) for the transformer. A primary series capacitor and secondary parallel capacitor resonant (SPR) topology RIPT is adopted as shown in figure 1(a). Forward LEDs and Backward LEDs arrays are utilized in the alternating current operation. Compared with the SPR topology RIPT, a non-resonant (NR) topology RIPT is also discussed in this study as shown in figure 1(b). Figure 1(c) shows the rotary circle transformer. The rotary circle transformer consists of two layers. The top layer is spiral coils (20 turns) and the bottom layer is the ferrite (diameter 50 mm; depth 2 mm; material: NiZn). The primary inductance and secondary inductance are *Lp* and *Ls*. The mutual inductance is M (= L_m). The coupling coefficient (k) is defined as in (1).

$$k = \frac{M}{\sqrt{L_p L_S}} \tag{1}$$

The slip of the rotary circle transformer is defined as in (2)

$$\text{slip} = (f_{SW} - f_m) / f_{SW} \tag{2}$$

wher f_{SW} is the switching frequency of the transformer (v_{in}) and f_m is the mechanically rotary frequency of the transformer.

II. Transfer Function of the RIPT System

This study discusses the characteristics of the RIPT for LED lighting systems under varied air gap [6, 7], changed load, and so on. Figure 2 shows the equivalent circuits of the RIPT for LED lighting systems. The high frequency voltage v_{in} is generated by the DC-AC HBI. The equivalent load of the LEDs considering rotary effect is simplified as R_L/slip (=R_{LS}). The primary series capacitor and secondary parallel capacitor are Cp and Cs. The primary resistance and secondary resistance of the spiral coils are r_P and r_S. The mutual inductance is M (=L_m), the equivalent resistance of rotary transformer is R_m. The primary leakage inductance and secondary leakage inductance are L_{lp} and L_{ls}.

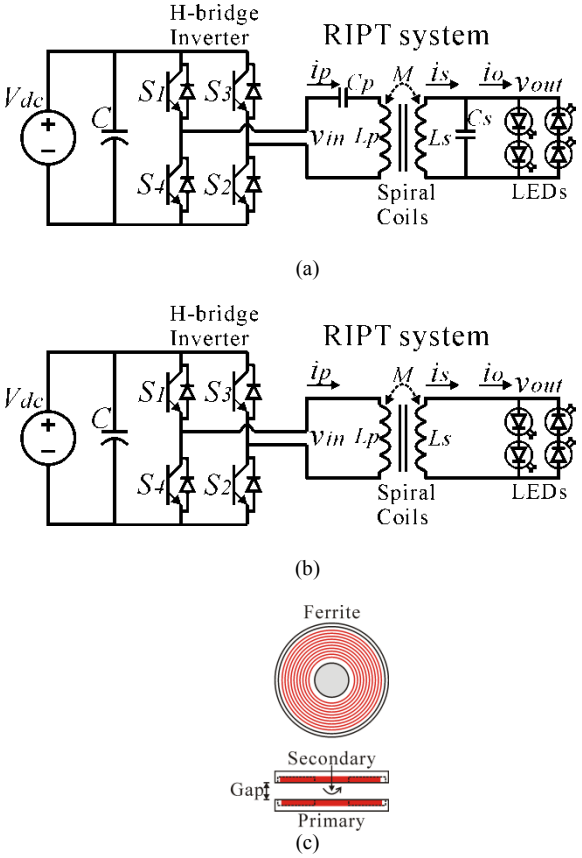

Fig. 1. Rotary inductive power transfer for LED lighting systems (a) SPR topology (b) NR topology (c) rotary circle transformer.

A. Transfer Function of SPR Topology

The transfer function of the SPR topology RIPT for LED lighting system is simplified as two zeros (s = 0, 0) and five poles as in (3).

$$\frac{v_{out}(s)}{v_{in}(s)} = \frac{s^2 \times C_p \times L_m \times R_{LS} / [R_m \times (R_{LS} + r_S)]}{(1+\frac{s}{p_H}) \times (1+\frac{2\zeta_1}{\omega_{n1}} s + \frac{s^2}{\omega_{n1}^2}) \times (1+\frac{2\zeta_2}{\omega_{n2}} s + \frac{s^2}{\omega_{n2}^2})} \tag{3}$$

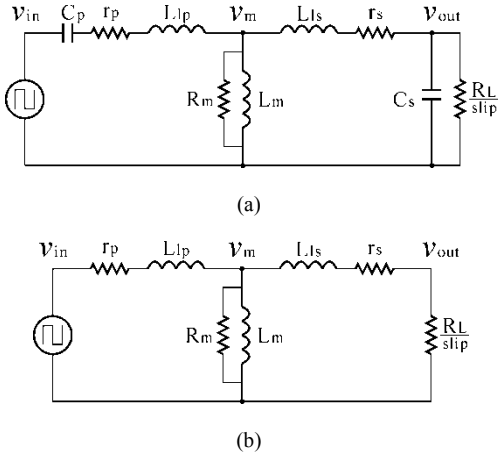

Fig. 2. Equivalent circuits of the RIPT for LED lighting systems (a) SPR topology (b) NR topology.

The high frequency pole (s = -p_H) is defined as in (4).

$$p_H = R_m \times (\frac{1}{L_{lp}} + \frac{1}{L_{ls}} + \frac{1}{L_m}) \quad (4)$$

The low frequency complex-conjugate poles (s = -p_{11} , -p_{12}) are as in (5).

$$1 + \frac{2\zeta_1}{\omega_{n1}} s + \frac{s^2}{\omega_{n1}^2} = 0 \Rightarrow s = -(\zeta_1 \pm j\sqrt{1-\zeta_1^2})\omega_{n1} \quad (5)$$

The damping ratio ζ_1 , natural undamped frequency ω_{n1} and resonant frequency ω_{r1} are as in (6).

$$\zeta_1 = r_p C_p \omega_{n1} / 2$$
$$\omega_{n1}^2 = 1 / C_p (L_{lp} + L_m)$$
$$\omega_{r1} = \sqrt{1-\zeta_1^2}\ \omega_{n1} \quad (6)$$

The middle frequency complex-conjugate poles (s = -p_{21} , -p_{22}) are as in (7).

$$1 + \frac{2\zeta_2}{\omega_{n2}} s + \frac{s^2}{\omega_{n2}^2} = 0 \Rightarrow s = -(\zeta_2 \pm j\sqrt{1-\zeta_2^2})\omega_{n2} \quad (7)$$

The damping ratio ζ_2 , natural undamped frequency ω_{n2} and resonant frequency ω_{r2} are as in (8).

$$\zeta_2 = 1/2R_{LS}C_S\omega_{n2}$$
$$\omega_{n2}^2 = (1 + r_S / R_{LS}) / C_S (L_{ls} + \frac{L_{lp}L_m}{L_{lp} + L_m})$$
$$\omega_{r2} = \sqrt{1-\zeta_2^2}\ \omega_{n2} \quad (8)$$

B. Transfer Function of NR Topology

The transfer function of the NR topology RIPT for LED lighting system is simplified as one zero (s = 0) and three poles as in (9).

$$\frac{v_{out}(s)}{v_{in}(s)} = \frac{s \times L_m \times R_{LS} / [r_P \times (R_{LS} + r_S)]}{(1 + \frac{s}{p_H}) \times (1 + \frac{s}{p_m}) \times (1 + \frac{s}{p_l})} \quad (9)$$

The pole (s = -p_H) operates at the high frequency domain as in (10).

$$p_H = R_m \times (\frac{1}{L_{lp}} + \frac{1}{L_{ls}} + \frac{1}{L_m}) \quad (10)$$

The pole (s = -p_m) operates at the middle frequency domain as in (11).

$$p_m = \frac{(L_{lp} + L_m) \times (r_S + R_{LS})}{L_{lp}L_{ls} + L_{lp}L_m + L_{ls}L_m} \quad (11)$$

The pole (s = -p_l) operates at the low frequency domain as in (12).

$$p_l = r_P / (L_{lp} + L_m) \quad (12)$$

According to (3) and (9), there are two pairs of resonant poles in the SPR topology RIPT system and three non-resonant poles in the NR topology RIPT system [8].

III. Experimental Results

Figure 3 shows the test bench of the rotary inductive power transfer for LED lighting systems. The parameters of the RIPT for LED lighting system are as follow: DC bus voltage Vdc is 24V; Lp and Ls are 25 μH; r_P and r_S are 0.2 Ω; R_L is 100 Ω; Cp and Cs are 0.1 μF; oscillation frequency is 100 kHz ($\omega_o = 1/\sqrt{L_S C_S}$; $f_o = \omega_o/2\pi$).

Figure 4 shows the frequency response of the SPR topology RIPT system operated at f_m (=0.5Hz). As shown in figure 4(a), the resonant frequency ω_{r1} and ω_{r2} move to each other and meet at oscillation frequency (ω_o) as air gap increased from 2mm to 4mm and 6mm; the output voltage is increasing as the air gap increasing. As shown in figure 4(b) and 4(c), the input-output powers are increasing as the air gap increasing. As shown in figure 4(d), the efficiency of the SPR topology operated at frequency ($f_{SW} = f_o$) are 82.4% (gap: 2mm), 83.4% (gap: 4mm), and 85.9% (gap: 6mm), respectively. The specification of the SPR topology RIPT system with varied air gap is given in table I (f_m: 0.5 Hz).

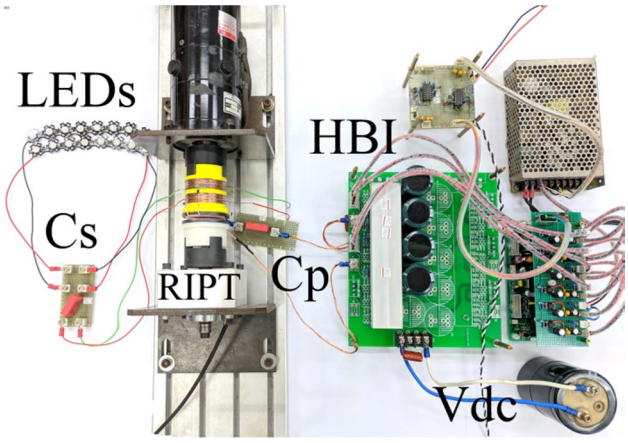

Fig. 3. Test bench of the rotary inductive power transfer for LED lighting systems.

TABLE I
SPECIFICATION OF THE SPR TOPOLOGY RIPT SYSTEM WITH VARIED AIR GAP

Air Gap	2mm	4mm	6mm
$L_{lp} = L_{ls}$	6.25µH	10µH	12.5µH
Lm	18.75µH	15µH	12.5µH
k	0.75	0.6	0.5
f_{r1} ($\omega_{r1}/2\pi$)	60kHz v_{out}: 83.59 V_{rms}	68kHz v_{out}: 86.64 V_{rms}	74kHz v_{out}: 92.62 V_{rms}
f_{r2} ($\omega_{r2}/2\pi$)	183kHz v_{out}: 135.6V_{rms}	154 kHz v_{out}: 134.3 V_{rms}	141 kHz v_{out}: 131 V_{rms}
f_{SW} : 100kHz	v_{out}: 21.8 V_{rms} P_{in}: 5.73 W P_{out}: 4.72 W Eff.: 82.4 %	v_{out}: 26.8 V_{rms} P_{in}: 8.48 W P_{out}: 7.07 W Eff.: 83.4 %	v_{out}: 33.0 V_{rms} P_{in}: 12.44 W P_{out}: 10.70 W Eff.: 85.9 %

Figure 5 shows the frequency response of the NR topology RIPT for LED lighting system. As shown in figure 5(a), the output voltage is decreasing as air gap increased from 2mm to 4mm and 6mm (switching frequency f_{SW}: 60-180 kHz). As shown in figure 5(b), 5(c), and 5(d), the input-output powers and efficiency are decreasing as the air gap increasing. Figure 5(d) shows the efficiency of the NR topology operated at frequency (f_{SW} = 100 kHz) are 97.6% (gap: 2mm), 96.3% (gap: 4mm), and 93.9% (gap: 6mm), respectively. The specification of the NR topology RIPT system with varied air gap is given in table II (f_m : 0.5 Hz).

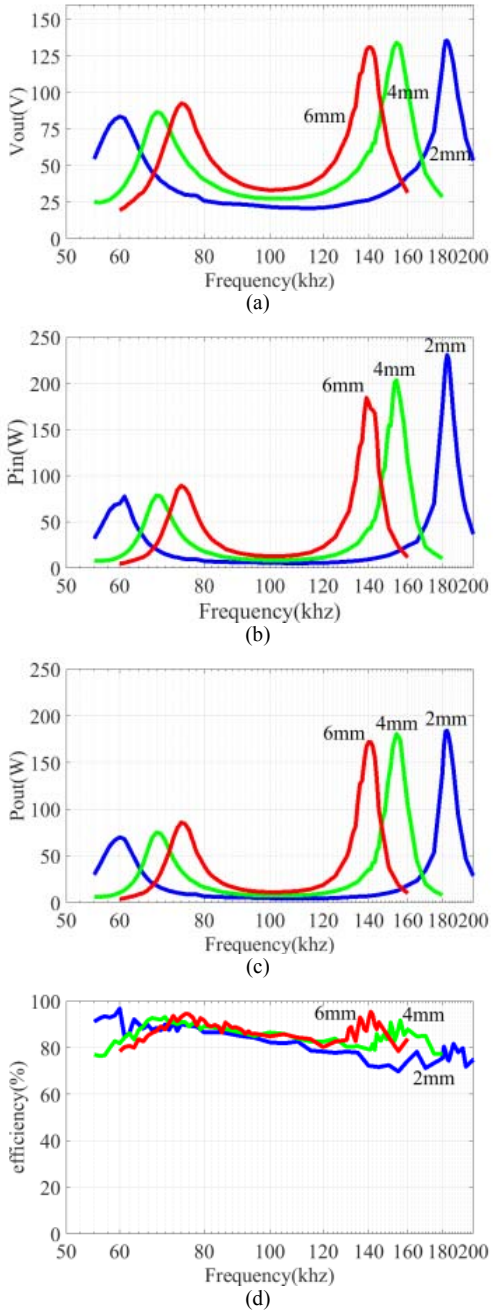

Fig. 4. Frequency response of the SPR topology RIPT system operated at f_m (= 0.5 Hz) (test results)for LED lighting systems (a) output voltage (b) input power (c) output power (d) efficiency.

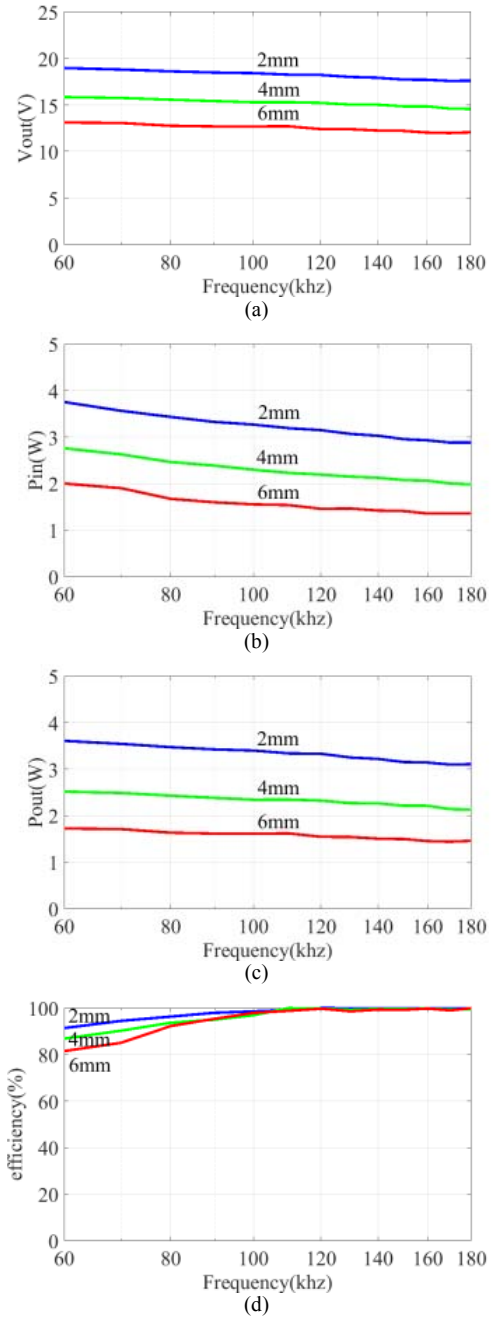

Fig. 5. Frequency response of the NR topology RIPT system operated at f_m (= 0.5 Hz) (test results)for LED lighting systems (a) output voltage (b) input power (c) output power (d) efficiency.

TABLE II
SPECIFICATION OF THE NR TOPOLOGY RIPT SYSTEM WITH VARIED AIR GAP

Air Gap	2mm	4mm	6mm
$L_{lp} = L_{ls}$	6.25μH	10μH	12.5μH
Lm	18.75μH	15μH	12.5μH
k	0.75	0.6	0.5
P_l	1.3 kHz	1.3 kHz	1.3 kHz
P_m	1455 kHz	994 kHz	848 kHz
f_{SW} : 100kHz	v_{out}: 18.6 V_{rms} P_{in}: 3.47 W P_{out}: 3.38 W Eff.: 97.6 %	v_{out}: 16.0 V_{rms} P_{in}: 2.59 W P_{out}: 2.49 W Eff.: 96.3 %	v_{out}: 13.1 V_{rms} P_{in}: 1.79 W P_{out}: 1.68 W Eff.: 93.9 %

As shown in figure 4 and 5, the SPR and NR topologies are utilized to operate at the tightly coupled (k > 0.5) condition and enhance the performances of the RIPT for LED lighting system.

Figure 6 shows the SPR topology RIPT system operated at oscillation frequency ($f_{SW} = f_o$ = 100 kHz; f_m = 0.5Hz) under varied load (50-500Ω). The input power, output power, and efficiency of the SPR topology RIPT system are decreased as the load resistance (R_L) value increased. The output voltages are 21.8-22.2V (gap: 2mm), 26.6-27.1V (gap: 4mm), and 32.7-33.2V (gap: 6mm) under varied load (50-500Ω). The output voltages are slightly affected by varied load and are influenced by varied gap ($f_{r1} < f_{SW} < f_{r2}$).

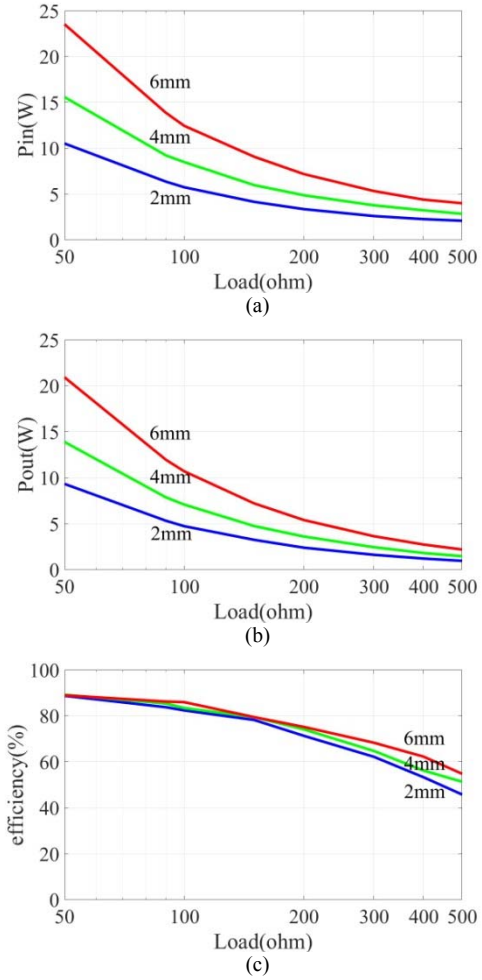

Fig. 6. SPR topology RIPT system operated at oscillation frequency ($f_{SW} = f_o$ = 100 kHz; f_m = 0.5 Hz) under varied load (test results). (a) input power (b) output power (c) efficiency.

Figure 7 shows the NR topology RIPT system operated at f_{SW} (= 100 kHz) under varied load (50-500Ω).The input power, output power, and efficiency of the NR topology RIPT system are decreased as the load resistance (R_L) value increased. The output voltages are 18.1-19.0V (gap: 2mm), 15.2-16.4V (gap: 4mm), and 12.5-13.8V (gap: 6mm) under varied load (50-500Ω).

As shown in figure 6 and 7, the NR topology RIPT system exhibits higher efficiency than SPR topology RIPT system.

Figure 8 shows the output voltage and current of the SPR topology RIPT for LED lighting system under low rotary velocity (f_{SW}: 100 kHz; f_m: 0.5Hz). The output voltage (v_{out}) is a high frequency sinusoidal wave with amplitude 30V. The forward LEDs current (i_{of}) and backward LEDs current (i_{ob}) are half cycle triangular wave with amplitude 0.8A as $|v_{out}| > 18$V. To keep the output voltage (v_{out}) coincident, the Vdc is decreased from 24V (gap: 2mm) to 20V (gap: 4mm) and 16V (gap: 6mm).

Figure 9 shows the output voltage and current of the NR topology RIPT for LED lighting system under low rotary velocity (f_{SW}: 100 kHz; f_m: 0.5Hz). The output voltage (v_{out}) is a high frequency square wave with amplitude 18.5V.

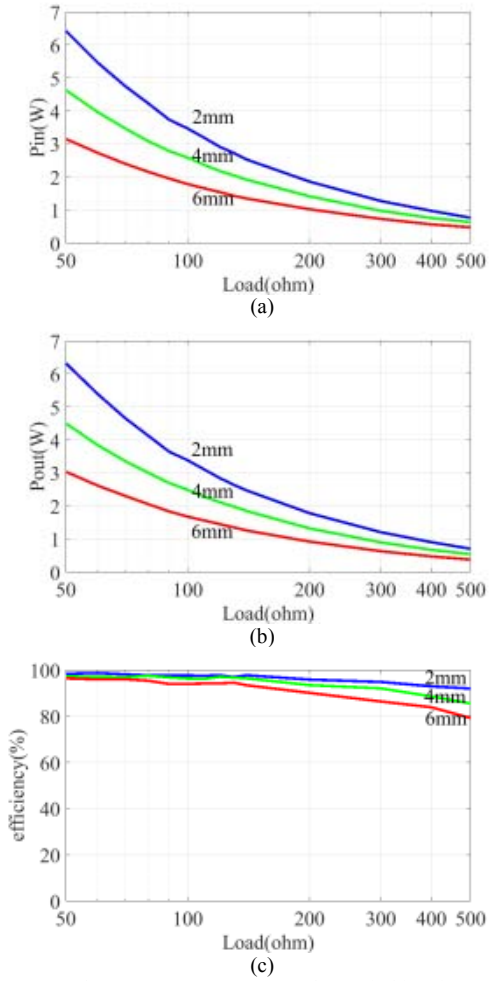

Fig. 7. NR topology RIPT system operated at switching frequency (f_{SW} = 100 kHz; f_m = 0.5 Hz) under varied load (test results). (a) input power (b) output power (c) efficiency.

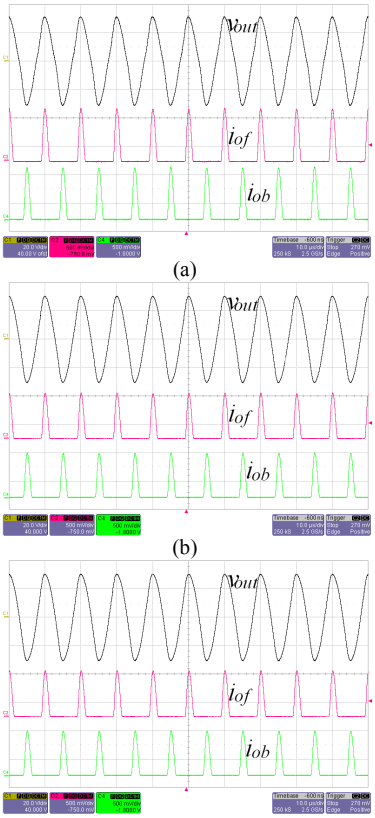

Fig. 8. Output voltage and current of the SPR topology RIPT for LED lighting system (f_{SW}: 100 kHz; f_m: 0.5 Hz; V_{out}: 20V/div.; i_{of} , i_{ob} : 0.5A/div.) (a) gap is 2mm and Vdc is 24V (b) gap is 4mm and Vdc is 20V (c) gap is 6mm and Vdc is 16V.

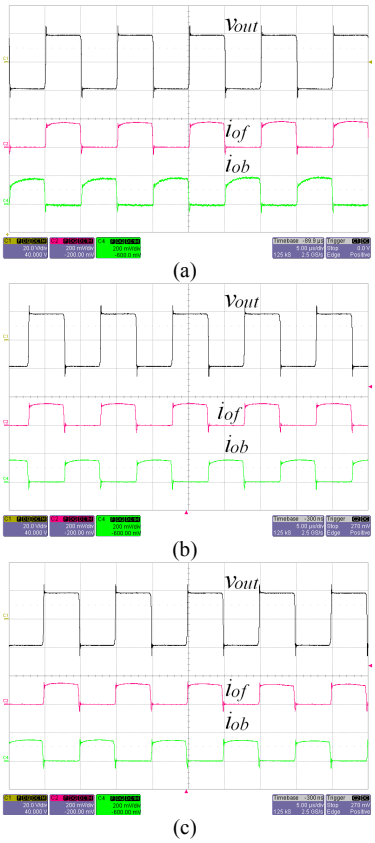

Fig. 9. Output voltage and current of the NR topology RIPT for LED lighting system (f_{SW}: 100 kHz; f_m: 0.5 Hz; V_{out}: 20V/div.; i_{of} , i_{ob} : 0.2A/div.) (a) gap is 2mm and Vdc is 24V (b) gap is 4mm and Vdc is 27V (c) gap is 6mm and Vdc is 33V.

The forward LEDs current (i_{of}) and backward LEDs current (i_{ob}) are half cycle square wave with amplitude 0.16A. To keep the output voltage (v_{out}) coincident, the Vdc is increased from 24V (gap: 2mm) to 27V (gap: 4mm) and 33V (gap: 6mm).

Figure 10 shows the output voltage and current of the SPR topology RIPT for LED lighting system under middle rotary velocity (f_{SW}: 100 kHz; f_m: 10 Hz). The output voltage (v_{out}) is a high frequency sinusoidal wave with amplitude 30V. The forward LEDs current (i_{of}) and backward LEDs current (i_{ob}) are half cycle triangular wave with amplitude 0.8A as $|v_{out}| > 18V$. To keep the output voltage (v_{out}) coincident, the Vdc is decreased from 24V (gap: 2mm) to 20V (gap: 4mm) and 16V (gap: 6mm).

As shown in figure 8 and 10, the output voltage and current waveforms of the SPR topology RIPT for LED lighting system are coincided under low rotary velocity and middle rotary velocity.

Figure 11 shows the output voltage and current of the NR topology RIPT for LED lighting system (f_{SW}: 100 kHz; f_m: 10 Hz). The output voltage (v_{out}) is a high frequency square wave with amplitude 18.5V. The forward LEDs current (i_{of}) and backward LEDs current (i_{ob}) are half cycle square wave with amplitude 0.16A. To keep the output voltage (v_{out}) coincident, the Vdc is increased from 24V (gap: 2mm) to 27V (gap: 4mm) and 33V (gap: 6mm).

As shown in figure 9 and 11, the output voltage and current waveforms of the NR topology RIPT for LED lighting system are coincided under low rotary velocity and middle rotary velocity.

As shown in figure 8, 9, 10, and 11, the NR topology RIPT scheme exhibits higher efficiency than SPR topology RIPT scheme for LEDs lighting system.

IV. Conclusions

This study measures the characteristics of the RIPT for LED lighting system under varied air gap, changed load, and so on. The transfer functions of the SPR topology and NR topology RIPT systems are derived and the frequency responses are coincided with the experimental results. In SPR topology, the input power and output power are increasing as the air gap increased. In NR topology, the input power, output power, and efficiency are decreasing as the air gap increased. Therefore, to keep the output voltage coincident, the DC bus voltage is decreased as gap is increased in SPR topology and the DC bus voltage is increased as gap is increased in NR topology. The detail experimental results are presented to demonstrate the performances of the proposed scheme.

Acknowledgment

This work was supported by the Ministry of Science and Technology of the R.O.C. under contract number MOST 107-2221-E-216-003.

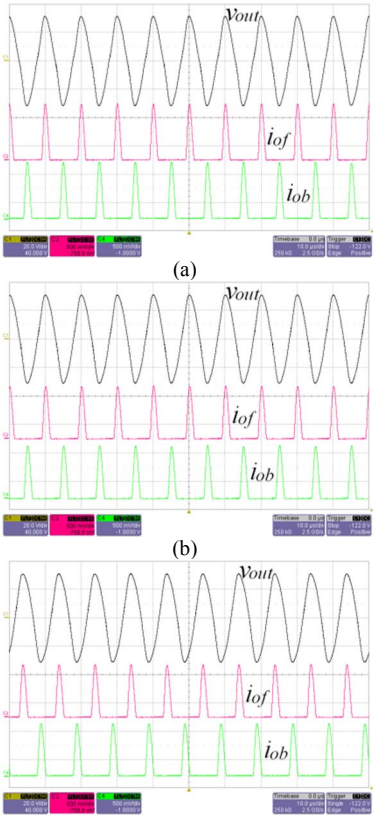

Fig. 10. Output voltage and current of the SPR topology RIPT for LED lighting system under middle rotary velocity (f_{SW}: 100 kHz; f_m: 10 Hz; V_{out}: 20V/div.; i_{of} , i_{ob} : 0.5A/div.) (a) gap is 2mm and Vdc is 24V (b) gap is 4mm and Vdc is 20V (c) gap is 6mm and Vdc is 16V.

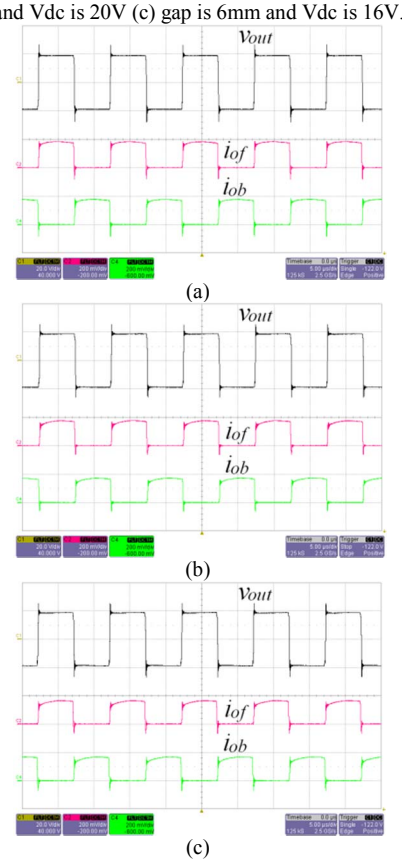

Fig. 11. Output voltage and current of the NR topology RIPT for LED lighting system under middle rotary velocity (f_{SW}: 100 kHz; f_m: 10 Hz; V_{out}: 20V/div.; i_{of} , i_{ob} : 0.2A/div.) (a) gap is 2mm and Vdc is 24V (b) gap is 4mm and Vdc is 27V (c) gap is 6mm and Vdc is 33V.

REFERENCES

[1] Konstantinos D. Papastergiou and D. Ewen Macpherson, "An airborne radar power supply with contactless transfer of energy—Part I: rotating transformers," *IEEE Trans. on Industrial Electronics*, vol.54, no.5, pp.2874-2884, Oct. 2007.

[2] M. Ruviaro, F. Runcos, N. Sadowski, and I. M. Borges, "Analysis and test results of a brushless doubly fed inductive machine with rotary transformer," *IEEE Trans. on Industrial Electronics*, vol.59, no.6, pp.2670-2677, June 2012.

[3] Riccardo Trevisan and Alessandra Costanzo, "A 1-kW contactless energy transfer system based on a rotary transformer for sealing rollers," *IEEE Trans. on Industrial Electronics*, vol.61, no.11, pp.6337-6345, Nov. 2014.

[4] Ali Abdolkhani, Aiguo Patrick Hu, and Nirmal-Kumar C. Nair, "A double stator through-hole type contactless slipring for rotary wireless power transfer applications," *IEEE Trans. on Energy Conversion*, vol.29, no.2, pp.426-434, June 2014.

[5] Xiaohui Qu, Wei Zhang, Siu-Chung Wong, and Chi K. Tse, "Design of a current-source-output inductive power transfer LED lighting system," *IEEE Journal of Emerging and Selected Topics in Power Electronics*, vol.3, no.1, pp.306-314, March 2015.

[6] Cong Zheng, Hongbo Ma, Jih-Sheng Lai, and Lanhua Zhang, "Design considerations to reduce gap variation and misalignment effects for the inductive power transfer system," *IEEE Trans. on Power Electronics*, vol.30, no.11, pp.6108-6119, Nov. 2015.

[7] John M. Miller, Omer C. Onar, and Madhu Chinthavali, "Primary-side power flow control of wireless power transfer for electric vehicle charging," *IEEE Journal of Emerging and Selected Topics in Power Electronics*, vol.3, no.1, pp.147-162, March 2015.

[8] Chung-Chuan Hou, Bo-Yen Chen, Kuo-Jui Lee, Heng-Yuan Ku, Po-Chun Chang, and Tang-Jung Chen, "Resonant and non-resonant inductive power transfer systems based on planar spiral coils," in *Proc. IEEE IFEEC Conf.*, 2017, pp.428-433.